Supporting Information

A new rare-earth borate $Ba_3BiPbEuO(BO_3)_4$ and luminescent properties of the $Ba_3BiPbY_{1-x}Eu_xO(BO_3)_4$ phosphors

Xuean Chen[a,*], Ruru Bian[a], Weiqiang Xiao[b] and Xiaoyan Song[a]

[a]*Faculty of Materials and Manufacturing, Key Laboratory of Advanced Functional Materials, Ministry of Education of China, Beijing University of Technology, 100124 Beijing, China.*

E-mail:xueanchen@bjut.edu.cn

[b]*Beijing Key Laboratory of Microstructure and Property of Solids, Beijing University of Technology, 100124 Beijing, China*

Content

Table S1 Atomic coordinates and equivalent isotropic displacement parameters ($Å^2$) for $Ba_3BiPbEuO(BO_3)_4$.

Atoms	Wyck sites	Site symmetry	x	y	z	U_{eq}
Ba1	4f	C_{3v}	0.6667	0.3333	0.08912(4)	0.0138(3)
Ba2	2d	D_{3h}	0.6667	0.3333	0.2500	0.0213(5)
Bi1/Pb1	4e	C_{3v}	0.0000	0.0000	0.16879(4)	0.0377(4)
Eu1	2a	D_{3d}	0.0000	0.0000	0.0000	0.0074(3)
B1	4f	C_{3v}	0.3333	0.6667	0.0541(9)	0.015(3)
B2	4f	C_{3v}	0.3333	0.6667	0.1722(8)	0.013(3)
O1	12k	C_s	0.1875(11)	0.375(2)	0.0548(4)	0.0208(18)
O2	12k	C_s	0.039(2)	0.5195(12)	0.1720(3)	0.024(2)
O3	2b	D_{3h}	0.0000	0.0000	0.2500	0.021(4)

Note: Bi1/Pb1 has the composition $Bi_{0.5}Pb_{0.5}$. U_{eq} is defined as one third of the trace of the orthogonalized **U** tensor.

Table S2 Selected bond lengths (Å) and angles (°) for $Ba_3BiPbEuO(BO_3)_4$.

Ba1-O2 × 3	2.798(10)	Bi1/Pb1-O2 × 6	2.7228(8)
Ba1-O1 × 6	2.869(3)	Eu1-O1 × 6	2.279(10)
Ba2-O2 × 6	2.701(10)	B1-O1 × 3	1.372(11)
Ba2-O3 × 3	3.1353(1)	B2-O2 × 3	1.384(11)
Bi1/Pb1-O3	2.1399(11)		
O1-Eu1-O1 × 3	180.0(8)	O1-B1-O1 × 3	119.98(6)
O1-Eu1-O1 × 6	84.1(4)	O2-B2-O2 × 3	120.00(2)
O1-Eu1-O1 × 6	95.9(4)		

Table S3 Le Bail refinement results of $Ba_3BiPbY_{1-x}Eu_xO(BO_3)_4$ ($0 \le x \le 1$) using the software package TOPAS.

Eu^{3+} content	x=0	x=0.1	x=0.2	x=0.4	x=0.6	x=0.8	x =1.0
Space group	*P*6$_3$/*mmc*	*P*6$_3$/*mmc*	*P*6$_3$/*mmc*	*P*6$_3$/*mmc*	*P*6$_3$/*mmc*	*P*6$_3$/*mmc*	*P*6$_3$/*mmc*
a (Å)	5.41223(14)	5.41512(15)	5.41626(16)	5.42260(13)	5.4262(7)	5.42907(12)	5.42809(17)
c (Å)	26.0981(8)	26.1096(8)	26.1364(8)	26.2276(8)	26.285(3)	26.3217(7)	26.3430(9)
V ($Å^3$)	662.05(4)	663.05(4)	664.01(5)	667.89(4)	670.24(18)	671.89(4)	672.19(5)
R_p, %	3.03	2.99	2.77	3.03	2.69	2.87	2.54
R_{wp}, %	4.95	4.66	4.43	4.75	4.26	4.54	4.09
GOF	2.16	1.99	1.90	2.14	1.83	1.94	1.82

Table S4 The spectral data on the Pb^{2+} and Bi^{3+} luminescence in various inorganic hosts.

Host	λ_{exc} (nm)	λ_{ems} (nm)	Stokes shift (cm^{-1})	Ref.
$SrB_2O_4:Pb^{2+}$	270	363	9489	[S1]
$Sr_6YAl(BO_3)_6:Pb^{2+}$	277	371	9147	[S2]
$CaZr(BO_3)_2:Pb^{2+}$	250	415	15903	[S3]
$LiCaBO_3:Pb^{2+}$	265	296	3952	[S4]
BaB_2O_4: Pb^{2+}	240	370	14640	[S5]
CaB_2O_4: Pb^{2+}	254	325	8600	[S6]
$CaAl_2O_4:Pb^{2+}$	237	360	14416	[S7]
$LiBa_2B_5O_{10}:Pb^{2+}$	245	430	17560	[S8]
$Li_4SrCa(SiO_4)_2:Pb^{2+}$	249	290	5678	[S9]
$BaB_8O_{13}:Pb^{2+}$	230	360	15700	[S10]
$Sr_6YAl(BO_3)_6:Bi^{3+}$	325	422	7073	[S2]
$Li_4SrCa(SiO_4)_2:Bi^{3+}$	310	380	5942	[S9]
$BaLa_2ZnO_5:Bi^{3+}$	320	410	6860	[S11]
$LaInO_3:Bi^{3+}$	340	420	5602	[S12]
$CaZrO_3:Bi^{3+}$	320	390	5609	[S13]
$NaLuGeO_4:Bi^{3+}$	316	400	6646	[S14]
$MgAl_2O_4:Bi^{3+}$	335	400	4851	[S15]
$LaYO_3:Bi^{3+}$	330	493	10019	[S16]
$(Ba,Sr)_3Sc_4O_9:Bi^{3+}$	330	526	11292	[S17]
$Ca_3Bi(PO_4)_3:Bi^{3+}$	326	434	7633	[S18]

Note：the Stokes shift is defined as energy difference between the intensity maxima in the excitation and emission bands.

References

[S1] İ. Pekgözlü, H. Karabulut, Synthesis and Photoluminescence of Pb^{2+} Doped SrB_2O_4, *Inorg. Mater.*, 2009, **45**, 61–64.

[S2] R. Sankar, G.V.S. Rao, Luminescence studies on doped borates, $A_6MM'(BO_3)_6$, *J. Alloys. Compd.*, 1998, **281**, 126–136.

[S3] G. Blasse, S.J.M. Sas, W.M.A. Smit, Luminescent materials with dolomite structure, *Mater. Chem. Phys.*, 1986, **14**, 253–258.

[S4] İ. Pekgözlü, E. Erdoğmuş, S. Çubuk, A.S. Başak, Synthesis and photoluminescence of $LiCaBO_3$:M (M:Pb^{2+} and Bi^{3+}) phosphor, *J. Lumin*., 2012, **132**, 1394–1399.

[S5] A.B. Gawande, R.P. Sonekar, S. K. Omanwar, Photoluminescence Properties of Combustion Synthesized BaB_2O_4:Pb^{2+} Phosphor, *Combust. Sci. Technol.*, 2014, **186**, 1928–1935.

[S6] H. Witzmann, J. Buhrow, K. Müller, Zum emissionsvermogen blei-manganaktivierter kalziumboratphosphore ($CaO{\cdot}B_2O_3$-Pb, Mn), *Naturwissenschaften*, 1964, **51**, 103.

[S7] C.P. Joshi, S.V. Moharil, Luminescence of Pb^{2+} in some aluminates prepared by combustion synthesis, *Phys. Stat. Sol. (b)*, 2000, **220**, 985–989.

[S8] G.J. Dirksen, G. Blasse, Luminescence in the Pentaborate $LiBa_2B_5O_{10}$, *J. Solid State Chem.*, 1991, **92**, 591–593.

[S9] İ. Pekgözlü, E. Erdoğmuş, M. Yılmaz, Synthesis and photoluminescence properties of $Li_4SrCa(SiO_4)_2$: M (M: Pb^{2+} and Bi^{3+}), *J. Lumin.*, 2015, **161**, 160–163.

[S10] E. Erdoğmuş, E. Korkmaz, V.E. Kafadar, Luminescence of a novel near-UV emitting phosphor BaB_8O_{13}:Pb^{2+}, *J. Appl. Spectrosc.*, 2014, **80**, 945–949.

[S11] Y.S. Chang, Blue emitting phosphors of $BaLa_2ZnO_5$ activated by Bismuth ions, *J. Electrochem. Soc.*, 2011, **158**, J115–J119.

[S12] L.I. van Steensel, S.G. Bokhove, A.M. van de Craats, J. de Blank, G. Blasse, The luminescence of Bi^{3+} in $LaInO_3$ and some other perovskites, *Mater. Res. Bull.*, 1995, **30**, 1359-1362.

[S13] H. Witzmann, H. Anderson, D. Walther, Zur Lumineszenz wismutaktivierter Zirkondioxid-Calciumoxid-Phasen, *Zeitschrift für Physikalische Chemie*, 1968, **239**, 243-251.

[S14] W.X. Wang, Z.Y. Sun, X.Y. He, Y.D. Wei, Z.H. Zou, J.C. Zhang, Z.F. Wang, Z.Y. Zhang, Y.H. Wang, How to design ultraviolet emitting persistent materials for potential multifunctional applications: a living example of a $NaLuGeO_4$: Bi^{3+}, Eu^{3+} phosphor, *J. Mater. Chem. C*, 2017, **5**, 4310-4318.

[S15] W.A.I. Tabaza, H.C. Swart, R.E. Kroon, Optical properties of Bi and energy transfer from Bi to Tb in $MgAl_2O_4$ phosphor, *J. Lumin.*, 2014, **148**, 192–197.

[S16] D.R. Taikar, Sumedha Tamboli, S.J. Dhoble, Synthesis and photoluminescence properties of red, green and blue emitting $LaYO_3$:M (M = Eu^{3+}, Tb^{3+}, Sm^{3+},Bi^{3+}, Pb^{2+}) phosphors, *Optik*, 2017, **142**, 183-190.

[S17] P.P. Dang, S.S. Liang, G.G. Li, H.Z. Lian, M.M. Shang, J. Lin, Broadly color tuning of Bi^{3+}/Eu^{3+}-doped $(Ba, Sr)_3Sc_4O_9$ solid solution compounds *via* crystal field modulation and energy transfer, *J. Mater. Chem. C*, 2018, **6**, 9990–9999.

[S18] M.K. Sahu, M. Jayasimhadri, Conversion of blue emitting thermally stable $Ca_3Bi(PO_4)_3$ host as a color tunable phosphor via energy transfer for luminescent devices, *J. Lumin.*, 2020, **227**, 117570.

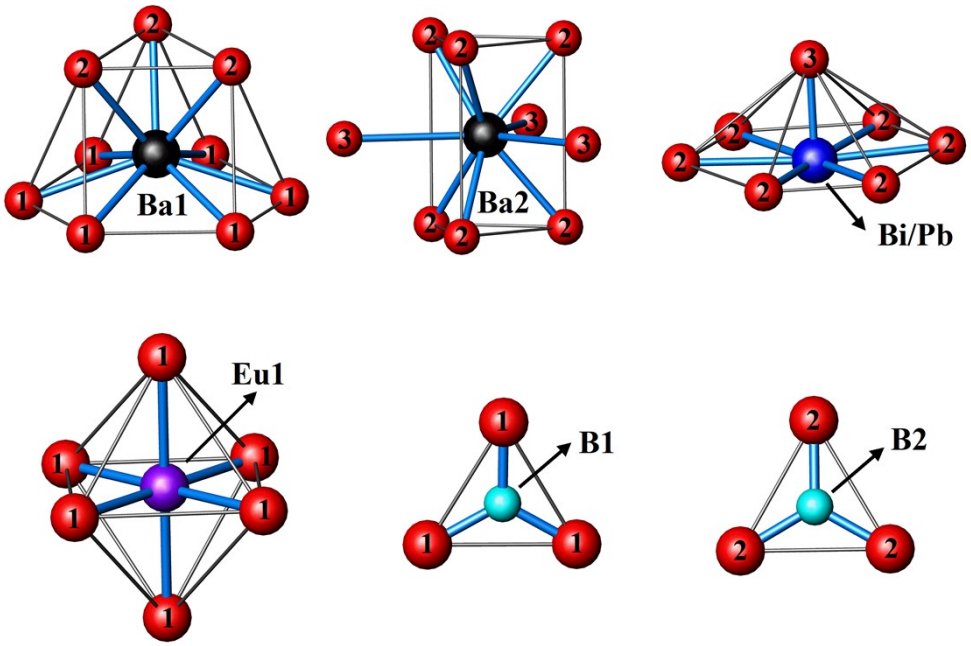

Fig. S1 The local environment of each cation site in $Ba_3BiPbEuO(BO_3)_4$ (the numbers correspond to the oxygen atom designations). Ba: black balls; Bi/Pb: blue balls; Eu: magenta balls; B: cyan balls; O: red balls.

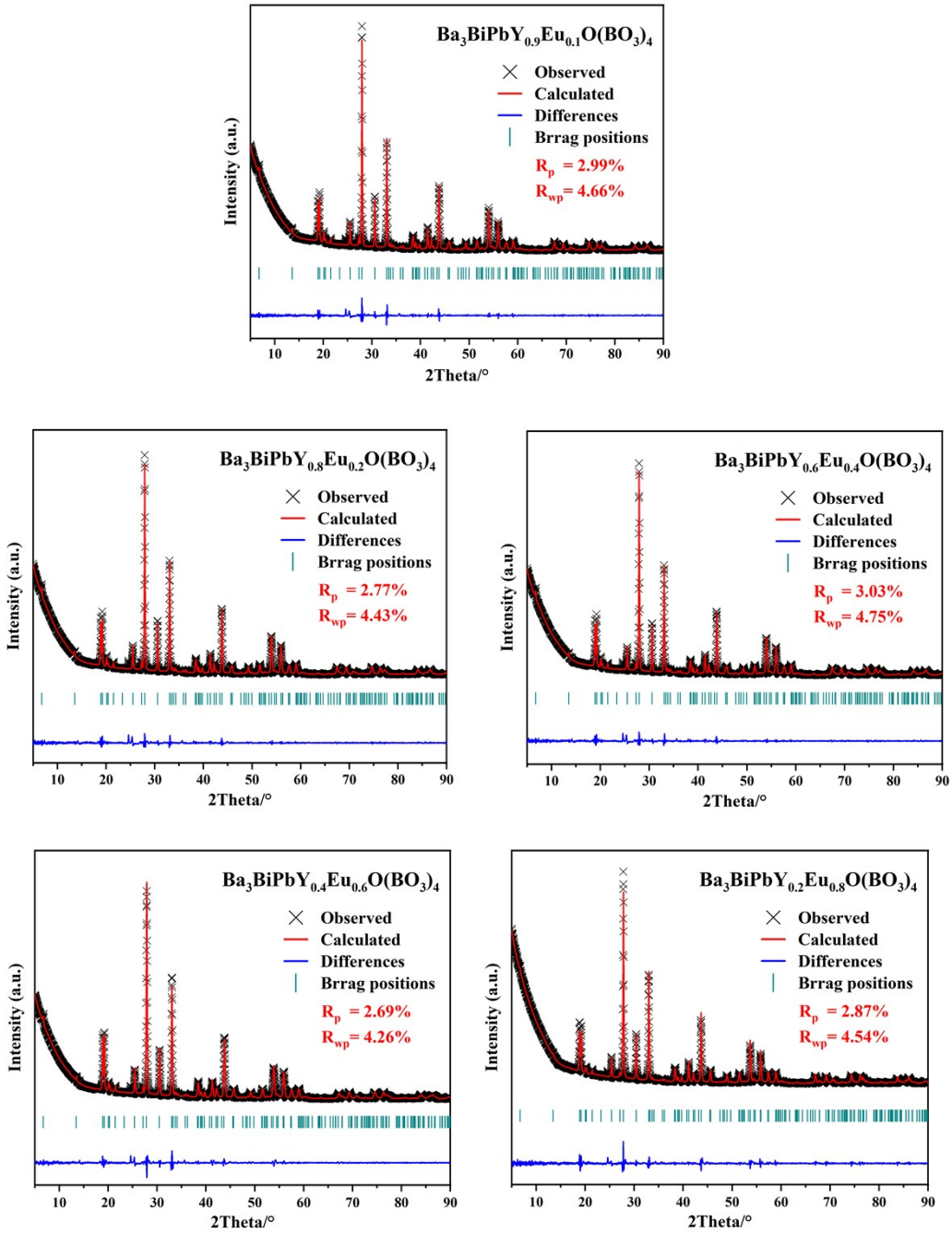

Fig. S2 Le Bail refinements of powder X-ray diffractograms of the $Ba_3BiPbY_{1-x}Eu_xO(BO_3)_4$ solid solutions (x = 0.1, 0.2, 0.4, 0.6 and 0.8).

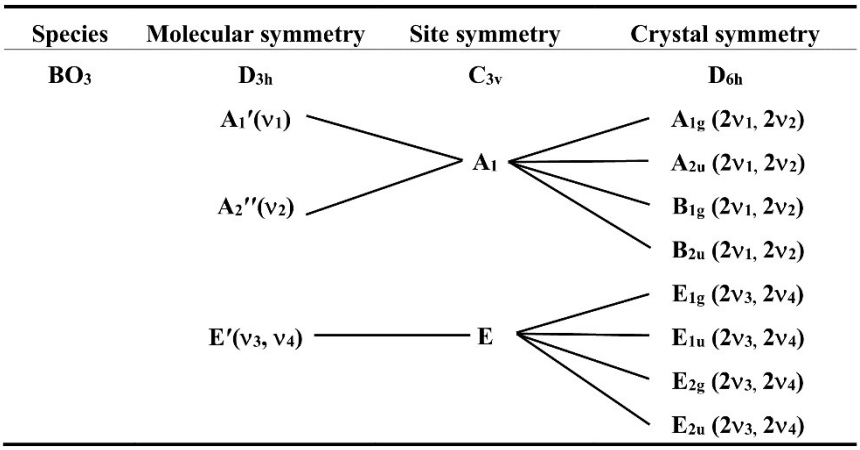

Fig. S3 Correlation diagram of the BO_3 internal vibrations in $Ba_3BiPbEuO(BO_3)_4$, space group $P6_3/mmc$

It is well-known that the free BO_3 unit with D_{3h} symmetry has 12 vibrational degrees of freedom, and its irreducible representations of the normal modes can be written as follows: $\Gamma_{BO3} = 1A_1' + 1A_2' + 2A_2'' + 3E' + 1E''$, where $1A_2'' + 1E'$ are translational modes, $1A_2' + 1E''$ are rotational modes, and the rest ($1A_1' + 1A_2'' + 2E'$) are internal modes.[46] $Ba_3BiPbEuO(BO_3)_4$ crystallizes in the hexagonal space group $P6_3/mmc$ (D_{6h}^4, no. 194), and its primitive cell comprises eight BO_3 units. Each B atom is surrounded by three oxygen atoms of the same type, so the BO_3 group is an equilateral triangle with site symmetry C_{3v} (see Table S1 and Fig. S1). In this case, the factor group analysis (see the correlation diagram in Fig. S3) predicts that the internal modes of the BO_3 units give rise to 48 lattice vibrations ($4A_{1g} + 4A_{2u} + 4B_{1g} + 4B_{2u} + 4E_{2u} + 4E_{2g} + 4E_{1u} + 4E_{1g}$). Similarly, we can deduce that 24 lattice vibrations ($2A_{1g} + 2A_{2u} + 2B_{1g} + 2B_{2u} + 2E_{2u} + 2E_{2g} + 2E_{1u} + 2E_{1g}$) originate from the translational modes of the BO_3 units, and 24 lattice vibrations ($2A_{1u} + 2A_{2g} + 2B_{1u} + 2B_{2g} + 2E_{2u} + 2E_{2g} + 2E_{1u} + 2E_{1g}$) from the rotational modes. The Ba atoms occupy two structure positions: 4f and 2d with C_{3v} and D_{3h} site symmetry, respectively. The disordered (Bi/Pb) and Eu atoms occupy positions 4e and 2a with C_{3v} and D_{3d} site symmetry, respectively. The O3 atom, that is an oxygen not bonded to B atoms, is located at the 2b Wyckoff site also with D_{3h} site symmetry. These atoms contribute totally with $2A_{1g} + 5A_{2u} + 4B_{1g} +$

$3B_{2u} + 3E_{2u} + 4E_{2g} + 5E_{1u} + 2E_{1g}$ translational modes. Summing all these modes and subtracting the acoustic modes ($A_{2u} + E_{1u}$), one gets the following optical vibrational modes of the crystal: $\Gamma_{opt} = 8A_{1g} + 2A_{1u} + 2A_{2g} + 10A_{2u} + 10B_{1g} + 2B_{1u} + 2B_{2g} + 9B_{2u} + 11E_{2u} + 12E_{2g} + 12E_{1u} + 10E_{1g}$, in which the $10A_{2u} + 12E_{1u}$ modes are IR-active, the $8A_{1g} + 12E_{2g} + 10E_{1g}$ modes are Raman-active, while the rest of the modes ($2A_{1u} + 2A_{2g} + 10B_{1g} + 2B_{1u} + 2B_{2g} + 9B_{2u} + 11E_{2u}$) are silent.

Furthermore, the internal vibrations of BO_3 units can be subdivided into: $\nu_1(2A_{1g} + 2A_{2u} + 2B_{1g} + 2B_{2u})$ – symmetric stretching, $\nu_2(2A_{1g} + 2A_{2u} + 2B_{1g} + 2B_{2u})$ – out-of-plane bending, $\nu_3(2E_{2u} + 2E_{2g} + 2E_{1u} + 2E_{1g})$ – antisymmetric stretching, and $\nu_4(2E_{2u} + 2E_{2g} + 2E_{1u} + 2E_{1g})$ – in-plane bending modes. Thus, the analysis shows that one expects to observe 12 modes in Raman and 8 modes in IR spectra for the BO_3 units, with the modes: $\nu_1(2A_{1g}) + \nu_2(2A_{1g}) + \nu_3(2E_{2g} + 2E_{1g}) + \nu_4(2E_{2g} + 2E_{1g})$ and $\nu_1(2A_{2u}) + \nu_2(2A_{2u}) + \nu_3(2E_{1u}) + \nu_4(2E_{1u})$, respectively. Here, E_{2g}, E_{1g}, and E_{1u} are twofold degenerated and often considered as one mode.

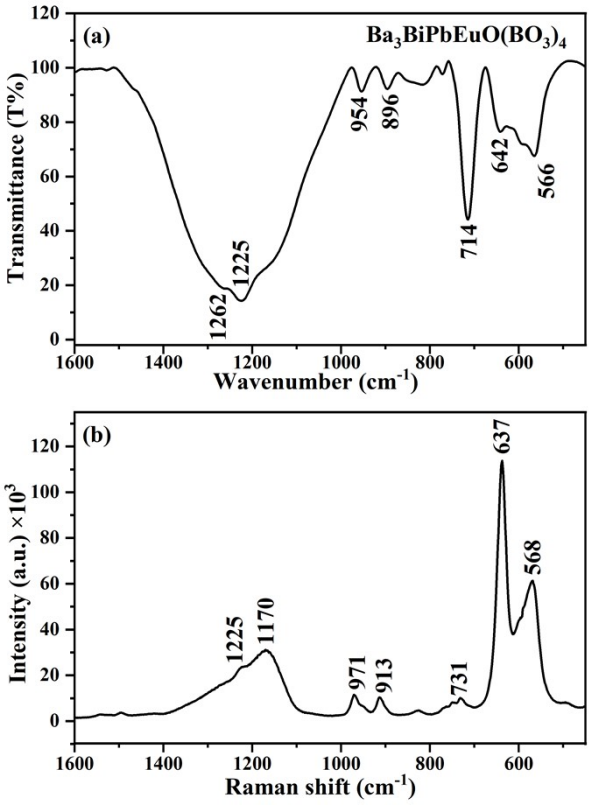

Fig. S4 Infrared (a) and Raman (b) spectra (excited by a 785 nm laser) of $Ba_3BiPbEuO(BO_3)_4$.

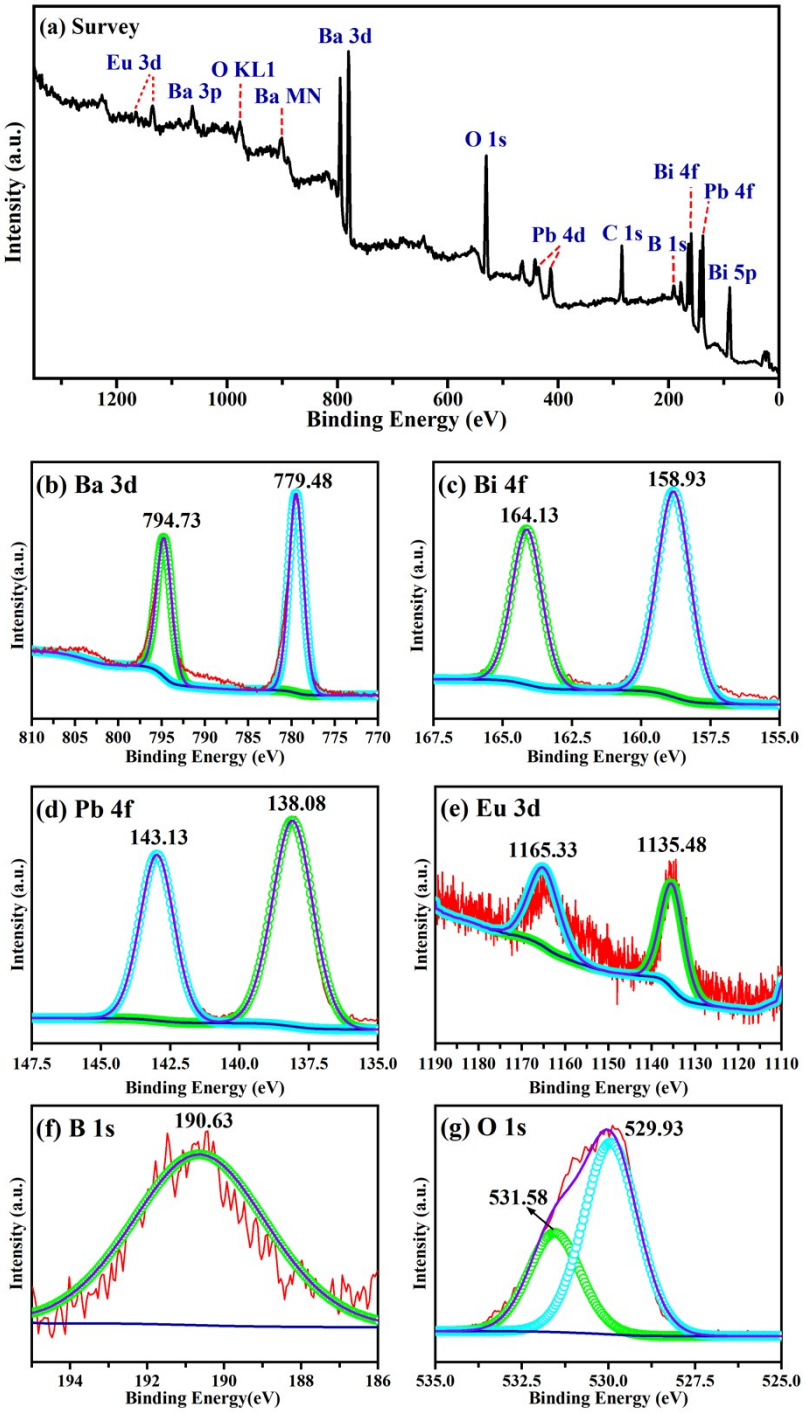

Fig. S5 Survey (a) and core-level spectra of Ba 3d (b), Bi 4f (c), Pb 4f (d), Eu 3d (e), B 1s (f), and O 1s (g) for $Ba_3BiPbEuO(BO_3)_4$.

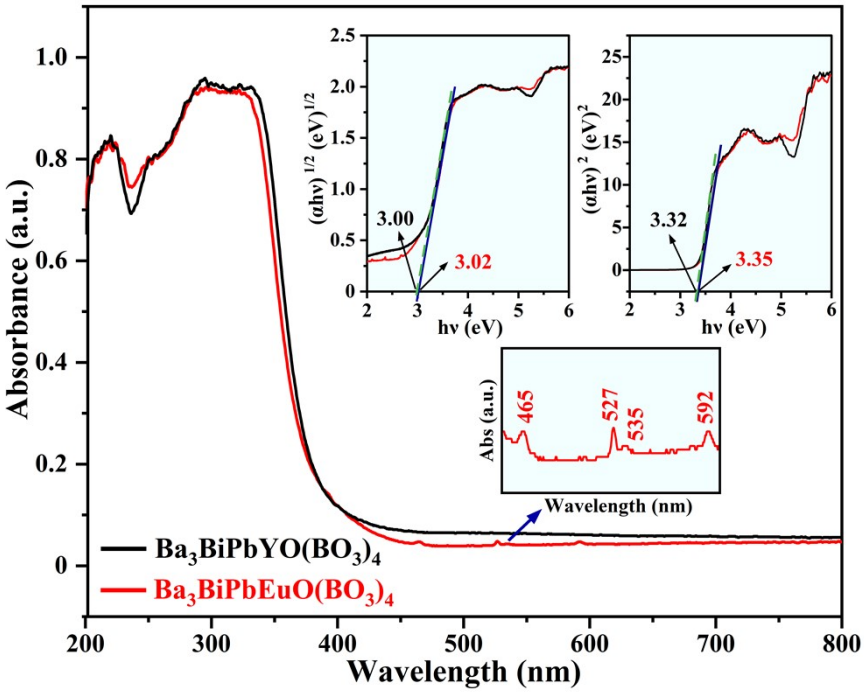

Fig. S6 UV–vis absorption spectrum of $Ba_3BiPbEuO(BO_3)_4$ as compared with that of $Ba_3BiPbYO(BO_3)_4$. The insets show the Tauc plots from indirect (left) and direct (right) transitions as well as local magnification of the UV–vis spectrum.

The optical band gap can be determined by the following Tauc formula:[64]

$$\alpha h\nu = A(h\nu - E_g)^n$$

where α, hν, A, and E_g stand for the absorption coefficient, photonic energy, proportionality constant, and band gap, respectively. The exponent n denotes the nature of the sample transition, $n = 1/2$ and 2 corresponding to direct and indirect allowed transitions, respectively. Here, we replace the absorption coefficient α with the absorbance obtained from UV–vis spectra and plot $(\alpha h\nu)^{1/n}$ as a function of hν. By extrapolating the linear part of the graphics to the axis of the abscissa, the indirect band gap of 3.02 eV and the direct band gap of 3.35 eV were obtained for $Ba_3BiPbEuO(BO_3)_4$, as shown in the insets of Fig. S6. For comparison, the UV–vis absorption spectrum of $Ba_3BiPbYO(BO_3)_4$ was also displayed in Fig. S6. It was observed that the optical band gaps of the undoped material, derived from the turning point of the absorption edge in the absorption spectrum, were around 3.00 eV for indirect and 3.32 eV for direct transitions, respectively, which are slightly less than the corresponding ones observed in its Eu-analog.

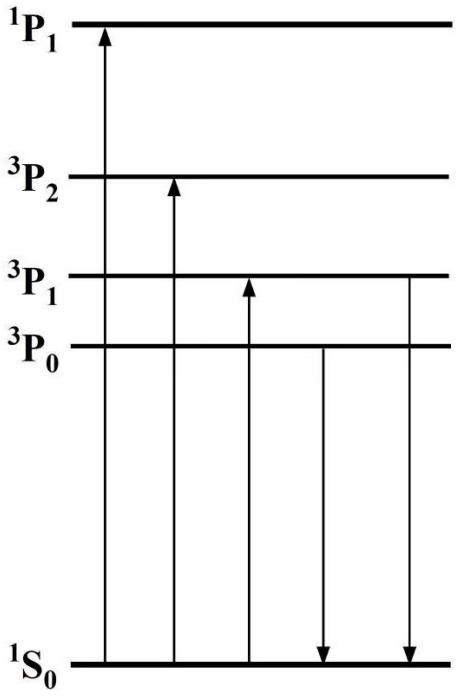

Fig. S7 Schematic representation of the energy level scheme of a free ion with ns^2 configuration (Pb^{2+}, Bi^{3+} etc.).

The ground state of the free Pb^{2+} and Bi^{3+} ions is $^1S_0$, while the 6s6p excited states give rise to the triplet levels ($^3P_0$, $^3P_1$, $^3P_2$) and the $^1P_1$ singlet state in sequence of energy increase (see Fig. S7). The lowest energy $^1S_0 \rightarrow ^3P_0$ transition is strongly forbidden, but the $^1S_0 \rightarrow ^3P_1$ and $^1S_0 \rightarrow ^3P_2$ transitions become more allowed due to spin–orbit coupling and coupling to asymmetrical phonon modes, respectively. The $^1S_0 \rightarrow ^1P_1$ transition is parity- and spin-allowed, but the $^1P_1$ state has higher energy than the $^3P_1$ state. The emission from the $^3P_1 \rightarrow ^1S_0$ transition is usually observed at room temperature, although the highly forbidden $^3P_0 \rightarrow ^1S_0$ emission is also observed at low temperatures.[65]

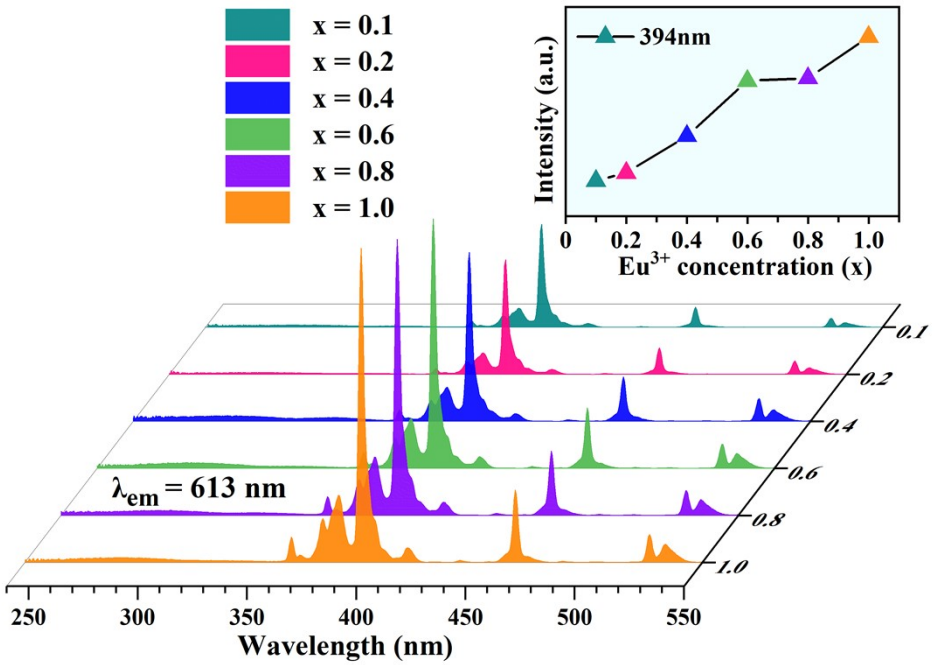

Fig. S8 PLE spectra of $Ba_3BiPbY_{1-x}Eu_xO(BO_3)_4$ ($0.1 \leq x \leq 1.0$) phosphors. Inset is the variation of 394 nm ($^7F_0 \rightarrow {}^5L_6$ of Eu^{3+}) excitation intensity.

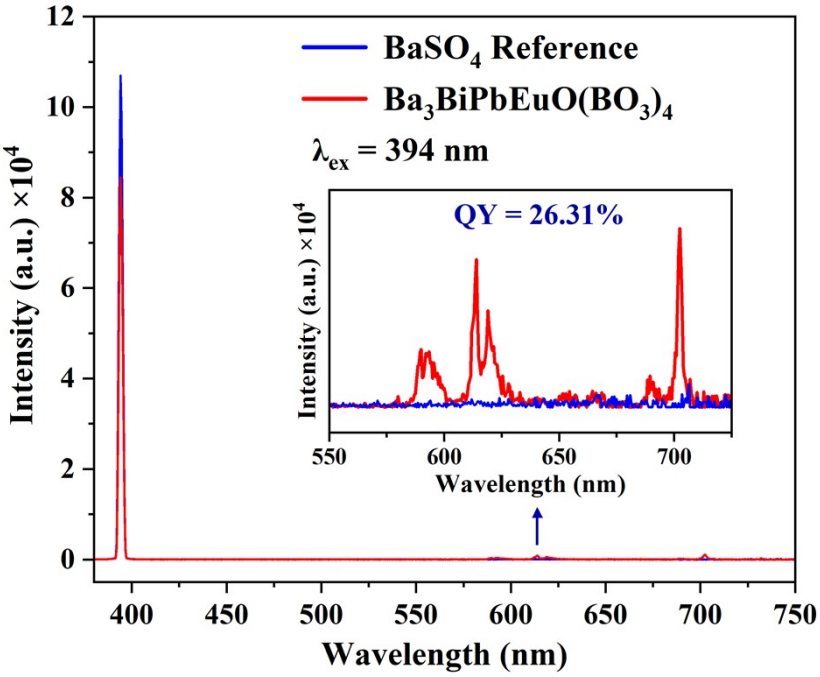

Fig. S9 Excitation line of $BaSO_4$ reference and the PL spectrum of the $Ba_3BiPbEuO(BO_3)_4$ phosphor collected using an integrating sphere (λ_{ex} = 394 nm); inset shows a local magnification of the PL spectrum.

The quantum yield (QY for short) can be determined by an integrated sphere method based on the following equation:

$$QY = \frac{\int L_S}{\int E_R - \int E_S}$$

Where $\int L_S$ is the integrated intensity of the PL spectrum for the sample, $\int E_R$ and $\int E_S$ are the integrated intensities of the PLE spectra for $BaSO_4$ powder and the sample, respectively.[79] The excitation line of white $BaSO_4$ powder and emission spectrum of the $Ba_3BiPbEuO(BO_3)_4$ phosphor collected in an integrating sphere (λ_{ex} = 394 nm) are presented in Fig. S9, where the QY is estimated to be about 26.31%. There are several ways to improve the QY property.[80] One is to co-dope various sensitizer and activator into the same host to increase the luminescence intensity through the energy transfer process. The other is to control the crystallite size or to explore alternative synthetic routes to reduce defects inducing non-radiative losses. We believe that the obtained QY value could be further enhanced by controlling the particle size, size distribution, morphology, and surface defects through optimization of the preparation conditions

and material compositions.